

- R. A. Berner (3)], and inhibition of methane production by dissolved sulfide [Th. E. Cappenberg, *Microbiol. Ecol.* 2, 60 (1975)].
6. Previous observations of anoxic conditions in Cape Lookout Bight were reported by R. Menzies, G. Rowe, and L. Atkinson [*Int. Rev. Gesamten Hydrobiol.* 53, 77 (1968)]. The organic-rich sediments accumulate in the bight as a result of decreases in current velocity of waters entering either through Barden Inlet or the open-ocean entrance bordering Shackelford Bank.
 7. P. E. Cloud [*Am. J. Sci.* 258A, 35 (1960)] has discussed the abiotic characteristics of "gas trackways" observed in modern and ancient carbonate sediments. The possibility that macrofauna occupy the bight interior during winter months has not been ruled out and it is conceivable that vacated burrow structures could be maintained by bubble ebullition during summer months. Small puffs of sediment accompanied many bubbles observed exiting bubble tubes.
 8. M. B. Goldhaber, R. C. Aller, K. Cochran, J. Rosenfeld, C. S. Martens, R. A. Berner, *Am. J. Sci.*, in press.
 9. M. B. Goldhaber, thesis, University of California, Los Angeles (1974).
 10. E. Sholkovitz, *Geochim. Cosmochim. Acta* 37, 2043 (1973). Centrifuge separation of interstitial waters from anoxic sediments was successfully used to study sulfate and other dissolved ions in the Santa Barbara Basin.
 11. The box corer was inserted by a diver. Its design and use are described by Goldhaber *et al.* (8).
 12. Kinetic reaction-diffusion models utilized to describe interstitial water distributions of sulfate can be found in R. A. Berner, in *The Sea*, E. D. Goldberg, Ed. (Wiley, New York, 1974) vol. 5, pp. 427-450; M. B. Goldhaber and I. R. Kaplan, in *ibid.*, pp. 569-655.
 13. The structure in the station 2 sulfate depth profile may be a relict feature from previous irrigation episodes.
 14. Methane concentrations in Cape Lookout Bight bottom waters averaged 40 $\mu\text{l/liter}$ during periods of active bubble transport in summer and early fall and 2 $\mu\text{l/liter}$ during the late fall, when bubbling had ceased.
 15. I thank F. Sansone and E. Powell for assistance with core collection, identification of macrofauna, and chemical analyses, and my colleagues in the Marine Sciences Program in Chapel Hill and at the Institute of Marine Sciences, Morehead City, for helpful information and discussions about the study site. D. Frankenberg, M. B. Goldhaber, L. K. Benninger, and R. C. Aller provided constructive critical reviews of the manuscript. Research supported by NSF grant DES75-06199 (Oceanography Section) and by a grant from the University of North Carolina Marine Sciences Council.

12 January 1976

Meteoroid Storms Detected on the Moon

Abstract. *Seismometers on the moon have detected several brief periods of enhanced meteoroid-impact activity, believed to represent encounters of the moon with "clouds" of objects in the kilogram range. The latest and most active encounter, in June 1975, is interpreted as a meteoroid cloud of diameter 0.1 astronomical unit and total mass 10^{13} to 10^{14} grams.*

Impacts of masses greater than about 50 g generate lunar seismic disturbances that are detected by the Apollo passive seismometer network. Thus, the moon

acts as a sounding board for meteoroids and the seismic data yield information on the mass and spatial distribution of these large particles in space. In this report we

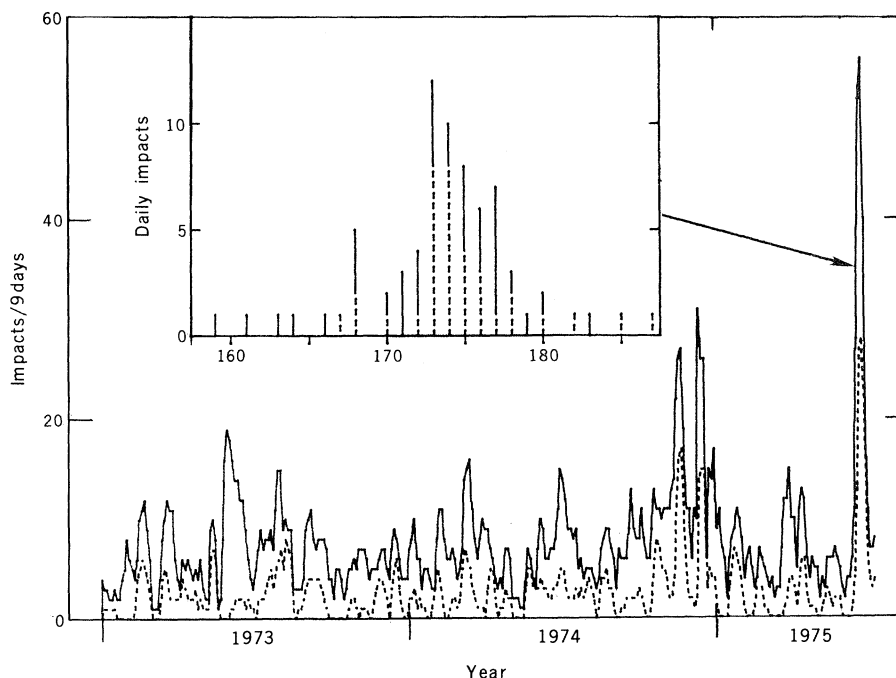


Fig. 1. Occurrence of meteoroid impacts detected by the Apollo seismic network. Each data point is the number of events in a 9-day window, with the window stepped 3 days per data point. The solid line represents all impacts and the dashed line represents only small impacts (see text). Shown in the inset are the daily numbers of impacts during the period from 7 June 1975 (day 158) to 6 July 1975 (day 187), which includes the most active interval. Solid and dashed lines are used as in the main figure. The data have been compiled from *Passive Seismic Experiment Long Period Event Catalog* (13).

describe time variations in the number of meteoroids hitting the moon. The large fluctuations observed suggest that some massive fragments are not randomly distributed in space, but are concentrated in clouds that sweep past the earth-moon system.

The passive seismic network, deployed by the Apollo astronauts, consists of four stations arranged in an approximately equilateral triangle 1100 km on a side with two stations 180 km apart at one corner. Each station consists of a set of three long-period (1 hertz and below) seismometers sensitive to motion in orthogonal directions and one short-period (1 hertz and above) seismometer sensitive to vertical motion. Each instrument can detect ground motions of about 0.05 nm at the peak of its response. A more detailed description of the instruments is found in Latham *et al.* (1).

The mass distribution of meteoroids has been measured by several earth-based methods (2), by satellite detectors (3), and from the lunar seismic data (1, 4). The latter yield mass distribution estimates that are lower by about an order of magnitude than those determined by earth-based methods. The mass distribution estimated by Duennebie and Sutton (5) from lunar short-period seismic data was very close to earth-based estimates in the mass range around 1 g. However, a correction in amplitude calibration for the Active Seismic Experiment (6) reduces their flux estimate by about an order of magnitude, making it an order of magnitude lower than the earth-based observations. In all known methods of meteoroid flux estimation, however, the parameter measured is difficult to relate to the mass of the impacting body.

Dainty *et al.* (7) used the lunar seismic data to determine the direction of approach of meteoroids in near-earth space. They concluded from studies of the variation in numbers of events observed as a function of phase of the moon that most meteoroid orbits lie near the plane of the ecliptic and that the orbits have aphelia between 2 and 5 A.U. In this report we note large temporal fluctuations in the numbers of impacts observed and interpret this observation in terms of the spatial distribution of meteoroids.

Between 1 January 1973 and 13 July 1975 (924 days), the long-period components of the passive seismometer array detected 815 signals interpreted as representing meteoroid impacts. These signals are similar to the signals from impacts of the lunar module and Saturn-rocket boosters. They differ from those

of moonquakes by their very emergent character and indistinct shear wave arrivals (7). Much of this character is due to the fact that impact-generated waves must traverse the surface scattering zone twice between the impact point and the seismometer, whereas waves generated by moonquakes with appreciable focal depth traverse it only once. Travel through the scattering zone causes the energy in the seismic wave train to be more diffused for impact signals than for moonquakes (8).

The history of impacts during the 924-day period is shown in Fig. 1. The solid line shows the number of impacts per 9-day period detected by the network and the dashed line shows the number of those which are believed to be small. An event is considered small if it is detected at only one corner of the triangular array and has detectable short-period energy, or if it is detected at the Apollo 12 station only, where the short-period seismometer is out of operation. From estimates of signal strength as a function of mass by Duennebier *et al.* (4), most of the small events represent masses from 50 to 10^3 g and the larger events represent masses between 5×10^3 and 5×10^4 g.

Of interest in Fig. 1 are several sharp peaks in activity, the three largest occurring in November and December 1974, and June 1975. Are such peaks expected occasionally in a random distribution? If meteoroids are scattered randomly in space, their impact times on the moon are randomly distributed throughout the observation period, and the number of observed impacts per unit time should follow a binomial distribution. For example, of 815 impacts observed during the 924 days (308 3-day intervals) the probability of observing x of them in a particular 3-day interval is

$$f(x) = \binom{815}{x} 308^{-x} (307/308)^{815-x} \quad (1)$$

where the combination sign

$$\binom{n}{x} = n!/x!(n-x)!$$

The frequency distribution of x impacts in any of the 308 intervals is given by $308 f(x)$. This distribution curve is compared with the observed occurrence of impacts in Fig. 2. The rightmost data clearly deviate from the theoretical curve (9). Indeed, any activity peak of 11 or more impacts in 3 days in this observation period of 924 days can be said to be unusual with 95 percent confidence. This implies that at least some objects of this size are not distributed randomly in space, but occur in clouds.

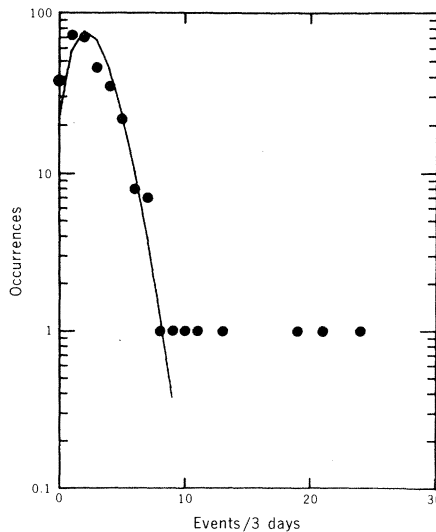


Fig. 2. Distribution of number of impacts observed in 3-day intervals from 1 January 1973 to 13 July 1975. The solid curve is the binomial distribution based on the assumption that all the impacts are random. The five most active intervals, which deviate significantly from the theoretical curve, occurred during the three most active periods of Fig. 1.

It could be argued that these events represent cometary particles such as those which produce the well-known yearly showers. Cometary particles, however, are normally much smaller (less than 1 g) than the particles detected by the seismometers (10). Also the lunar events show no yearly pattern and, indeed, no significant periodicity. Thus, these events are classified as sporadics, or meteoroids unrelated to known groups. Hoffman *et al.* (11) detected similar changes in meteoroid activity for masses less than 10^{-7} g. Their analysis of HEOS-2 satellite data suggests that some micrometeoroids (groups) have a lunar origin and others (swarms) a cometary origin.

The mass distribution also appears to vary. During the period of observation, 35 percent of the impacts observed were small by the criteria given earlier. During the three largest meteoroid storms, this percentage increased to about 58 percent. Thus the clouds appear to contain a larger percentage of small objects than does normal space.

The phase of the moon during high meteoroid activity is related to the possible orbit of the clouds. Both of the peaks late in 1974 occurred near new moon on consecutive months. Thus, the apparent motion of the cloud as viewed from the moon was toward the sun, since the seismic array is approximately centered on the front side of the moon. The peak in June 1975 occurred at full moon; thus, the apparent direction of motion was away from the sun. According to Dainty

et al. (7) most impacts are observed from these directions, implying orbits with aphelion distances between 2.8 and 5.0 A.U. (12).

It should be stressed that a cloud of meteoroids, as mentioned here, is very diffuse and is observed only because the moon is such a large detector. Peak activity corresponds to an infall rate of only one every 3 days over an area 100 km in radius. Thus, these clouds do not appear as meteoroid showers visible from the earth. The size of the cloud encountered in June 1975 can be estimated by assuming its velocity relative to the moon. If the velocity was about 20 km/sec, then, since the moon traversed the cloud in 10 days (Fig. 1, inset), the cloud is about 1.7×10^7 km in that dimension (~ 0.1 A.U.). We can estimate the density of the cloud by assuming a mass distribution for the detected objects. If the slope of the cumulative mass distribution curve is -1.23 (4), 18 percent of the mass in the observed range (50 g to 50 kg) is in the fraction with mass greater than 5 kg; meteoroids in this fraction are believed to be observable moonwide. During the 10-day interval of the June 1975 activity peak, 29 impacts believed to belong to this fraction were observed, with an estimated total mass of 320 kg. Thus, the total mass of impacting fragments in the range from 50 g to 50 kg is estimated to be 5.6 times this value, or 1800 kg. With the relative velocity assumed above, the moon swept out a volume of 1.6×10^{14} km³ in 10 days. Therefore, the density of the cloud averages about 10^{-8} g/cm³. Then, assuming that these particles are distributed evenly in a spherical cloud of diameter 1.7×10^7 km, the total mass of the cloud is estimated to be 10^{13} to 10^{14} g. This is equivalent to the mass of a spherical body of diameter 200 to 400 m and density 3 g/cm³.

It is interesting to estimate (with more certainty than in the mass calculation above) the probability of a collision between a space vehicle and one of the larger meteoroids in such a cloud. Assuming a cross section of about 1 km², a space station traveling at about 20 km/sec with respect to the cloud will meet one of these rocks (with unpleasant effects), on the average, once every 9000 years it spends within a cloud. Thus, a space station could expect more than reasonable security with a minimum of shielding.

In conclusion, the Apollo passive seismic experiment has detected massive meteoroids, not belonging to the well-known meteor showers, that do not hit the moon randomly, but occur in storms lasting from a few days to more than a

week. These storms represent extremely diffuse clouds that have previously gone undetected.

F. K. DUENNEBIER, Y. NAKAMURA
G. V. LATHAM, H. J. DORMAN
*Geophysics Laboratory, Marine Science
Institute, University of Texas,
Galveston 77550*

References and Notes

1. G. Latham *et al.*, *NASA Spec. Publ. SP-315* (1972), section 9.
2. G. S. Hawkins, *Annu. Rev. Astron. Astrophys.* **2**, 149 (1964); R. McCrosky, *Smithson. Astrophys. Obs. Spec. Rep.* **280** (1968).
3. P. M. Millman, *Moon* **8**, 228 (1973).
4. F. Duennebier *et al.*, in "Proceedings of the 6th Lunar Science Conference," *Geochim. Cosmochim. Acta* **2**, (Suppl. 6), 2417 (1975).
5. F. Duennebier and G. Sutton, *J. Geophys. Res.* **79**, 4365 (1974).
6. M. R. Cooper and R. L. Kovach, in "Proceedings of the 6th Lunar Science Conference,"

7. A. M. Dainty, S. Stein, M. N. Toksoz, *Geophys. Res. Lett.* **2**, 273 (1975).
8. G. Latham *et al.*, *NASA Spec. Publ. SP-272* (1971), p. 133.
9. It is also noted that the frequency of intervals of no impacts is significantly higher than theoretically expected. However, this may be due to high noise background near sunrises and sunsets, and resulting loss of signal detection.
10. B. C. Cour-Palais, *NASA Spec. Publ. SP-8013* (1969).
11. H. J. Hoffman, H. Fechtig, E. Grunn, J. Kissel, *Planet. Space Sci.* **23**, 985 (1975).
12. R. McCrosky, *Smithson. Astrophys. Obs. Spec. Rep.* **252** (1967).
13. F. Duennebier, D. Lammlein, G. Latham, J. Dorman, Y. Nakamura, *Passive Seismic Experiment Long Period Event Catalog* (Marine Science Institute, University of Texas, Galveston, 1975), vols. 1 to 6.
14. We wish to thank J. Lindsay and A. B. Ibrahim for reviewing the manuscript and offering constructive comments. Supported by NASA contract NAS 9-14581. Marine Science Institute Contribution No. 86.

15 January 1976; revised 8 March 1976

Tunneling in Ligand Binding to Heme Proteins

Abstract. *Rebinding of carbon monoxide to the beta chain of hemoglobin after photodissociation by a laser flash is intramolecular below about 200 K. Above 25 K, rebinding occurs via classical over-the-barrier motion; below, quantum-mechanical tunneling dominates. Both are described by an energy spectrum peaked at $E^{peak} = 4.0$ kilojoules per mole. The barrier width $d(E)$, determined from the energy dependence of the tunneling rate, depends on barrier height, $d(E) \approx 0.05$ nanometer $\times (E/E^{peak})^{1.5}$.*

Quantum-mechanical tunneling, in which a particle passes through a classically impenetrable barrier, plays a role even in polymers and biomolecules. Electron tunneling occurs in photosynthesis (1); molecular tunneling has been seen in the radiation-induced polymerization of formaldehyde (2). We report here the observation of molecular tunneling in the binding of carbon monoxide to the beta chain of hemoglobin (β Hb). Before describing our experiments, we make a few remarks concerning tunneling. Consider a molecule of mass M in thermal equilibrium with its surroundings at temperature T in a well B. Well B

shall be separated by a potential barrier of height E and width $d(E)$ from the deeper well A (Fig. 1a). The molecule can move from B to A by hopping over the barrier or tunneling through it (3). The two processes are distinguished by their temperature dependences. The classical Arrhenius (over-the-barrier) rate parameter k_a , given by

$$k_a(E) = A \exp(-E/k_B T) \quad (1)$$

vanishes in the limit $T \rightarrow 0$. Here, $k_B = 8.32$ joule mole⁻¹ K⁻¹ is the Boltzmann constant and 1 joule mole⁻¹ = 0.239 kcal mole⁻¹ = 0.010 eV. Quantum-mechanical tunneling can also be tem-

perature dependent, but in the limit $T \rightarrow 0$ remains finite and becomes temperature independent (4). Tunneling thus is established if the transition rate between two well-defined states becomes temperature independent as $T \rightarrow 0$. For a parabolic barrier with height $E \gg k_B T$, the low temperature limit can be written as

$$k_t(E) = A_t \exp[-\pi d(E) (2ME)^{1/2} / 2\hbar] \quad (2)$$

where the exponential is called the Gamow factor (5) and $2\pi\hbar$ is Planck's constant.

Experimentally we study the binding of ligands to heme proteins and heme model compounds by flash photolysis. The heme protein H with bound ligand L, HL, is placed in a cryostat and photodissociated by a laser flash. The subsequent rebinding, $H + L \rightarrow HL$, is followed optically with a transient analyzer with logarithmic time base that records from 2 μ sec to 1 msec in a single sweep (6). With this technique we previously investigated the binding of CO and O₂ to myoglobin (Mb) from 40 to 320 K (7). Extension of these experiments to 2 K gives evidence for tunneling in Mb and, in fact, in all systems where we looked (MbCO, MbNO, α HbCO, β HbCO, cytochrome P450 CO, carboxymethylcytochrome c CO, hydroxyheme CO, 2-methylimidazoleheme CO, and heme c octapeptide CO). For our work we selected β HbCO and prepared samples (in a mixture of glycerol and water, 3 : 1, by volume, pH 7.0) by the method of Geraci *et al.* (8).

Figure 1b gives rebinding curves for β HbCO. The quantity $N(t)$ is the fraction of Hb molecules that have not rebound CO at the time t after the laser flash (9). Since the curves extend over many orders of magnitude in time, $\log N(t)$ is plotted as a function of $\log t$. Figure 1c gives $N(t)$ for $T < 50$ K on an expanded scale. The curves display two conspicuous features: (i) Below about 20 K, they approach temperature independence; and (ii) $N(t)$ is not exponential, but close to a power law. To express feature (i), we characterize each curve in Fig. 1c by $t_{0.75}$, the time at which $N(t)$ drops from 1 to 0.75. The rate $k_{0.75} = 1/t_{0.75}$ is plotted in Fig. 2a versus $\log T$. Above 25 K, $k_{0.75}$ depends exponentially on T ; below 10 K, it is independent of T . Quantum-mechanical tunneling thus is established: Initial and final states in the transition are distinct as is proved by their optical spectra; the states are separated by a barrier as demonstrated by the Arrhenius behavior above 25 K, and the transition rate from B to A becomes temperature independent for $T \rightarrow 0$.

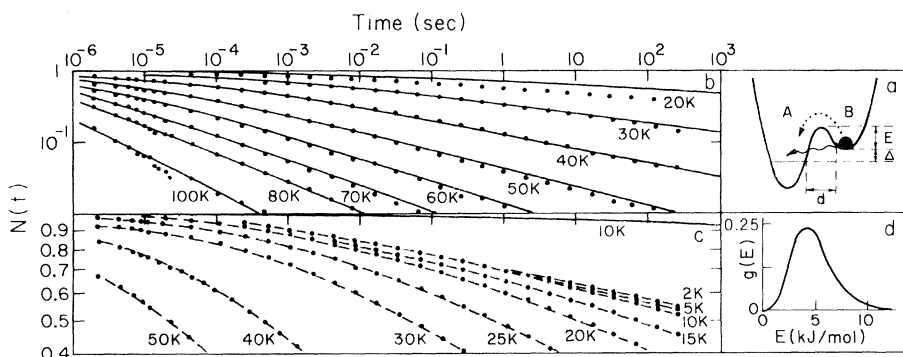


Fig. 1. (a) A molecule in well B can move to A by hopping over the barrier or tunneling through it. (b) Rebinding of CO to β Hb after photodissociation. $N(t)$ is the fraction of β Hb molecules that have not rebound CO at time t after the laser flash. (c) As (b), but with expanded $N(t)$ scale. The solid line labeled 10 K indicates $N(t)$ as expected without tunneling. (d) Activation energy spectrum for β HbCO. The solid lines in (b) are calculated with $g(E)$ as given here.